TURBULENT DISPERSION IN COASTAL ATMOSPHERIC BOUNDARY LAYERS: AN APPLICATION OF A LAGRANGIAN MODEL

YAPING SHAO

CSIRO Centre for Environmental Mechanics, Canberra, Australia

(Received in final form 6 November, 1991)

Abstract. A Lagrangian model is applied to simulate the dispersion of passive tracers (in particular, water vapour) in coastal atmospheric boundary layers under onshore wind conditions. When applied to convective boundary layers over uniform surfaces, the model gives results in agreement with those of similar studies. Numerical simulation of turbulent dispersion in coastal areas also reproduces the basic features known from experimental studies. Under onshore wind conditions, the humidity field is plume-shaped with the maximum vertical transport being over land downstream of the coast line. The model shows that the surface sensible heat flux over land, the static stability of the onshore air flow and the onshore wind speed are the most important factors determining the basic features of turbulent dispersion in coastal areas.

1. Introduction

In recent years, Lagrangian dispersion models have successfully predicted the distribution of air pollutants in both homogeneous and inhomogeneous turbulent air flows (e.g., Gifford, 1982; de Baas *et al.*, 1986; Sawford and Guest, 1987; Thomson, 1987; Luhar and Britter, 1989). These models, the basis of which is a simulation of tracer trajectories, naturally describe the movement of a pollutant and are numerically simple. Following Thomson (1987), the movement of a passive particle in a turbulent flow can be adequately described by a nonlinear stochastic equation system

$$\left.\begin{aligned} \mathrm{d}U_i &= a_i\,\mathrm{d}t + b_{ij}\,\mathrm{d}\xi_j \\ \mathrm{d}X_i &= U_i\,\mathrm{d}t \end{aligned}\right\}, \tag{1}$$

where U_i and X_i are the velocity and position of the particle, respectively; t is time; and $\mathrm{d}\xi_j$ is a random acceleration. The coefficients a_i and b_{ij} are determined by the structure of turbulence. Obviously, a prerequisite for the application of Lagrangian models is that the structure of turbulence is sufficiently understood. As a consequence of numerous theoretical and experimental studies, a relatively complete understanding of atmospheric turbulence over uniform surfaces has been achieved and this has provided a solid basis for the application of Lagrangian models. Boundary layers over nonuniform surfaces, however, are less well studied and this has so far been a major obstacle to the application of Lagrangian models in such conditions.

Based on airborne observations in the Upper Spencer Gulf (USG) region, South

Boundary-Layer Meteorology **59**: 363–385, 1992.

Australia, Shao and Hacker (1990) and Shao (1990) examined the structure of the coastal boundary layer. Three major conclusions were reached in those studies: (a) Coastal boundary layers under onshore wind conditions can be divided into an outer stable region over water and a growing transformed convective region over land, known as the thermal internal boundary layer (TIBL). The height of the TIBL can be approximated by Weisman's equation (Weisman, 1976; Stunder and Sethuraman, 1985). (b) While advection strongly affects the first-order parameters in boundary layers over nonuniform surfaces, the behaviour of some second- and higher-order moments is mainly determined by local forces. The influence of horizontal advection is secondary. (c) The behaviour of turbulence in the convective region is determined by three external parameters, namely, the surface heat flux over land, the onshore wind speed, and the static stability of the onshore airflow. These experimental results have increased the understanding of turbulence in coastal boundary layers and enabled the application of Lagrangian models to dispersion of passive tracers under such conditions.

In this study, the Lagrangian model suggested by Thomson (1987) is applied to simulate the dispersion of passive tracers (water vapour) in coastal areas under onshore wind conditions. The model predicts the distribution and vertical flux of tracer particles for given external conditions such as the surface heat flux over land and the stability of onshore airflow. For the implementation of the Lagrangian model, the observational results of the turbulent structure of coastal boundary layers obtained in the USG experiments are used.

2. Observational Evidence

Distribution and transport of passive tracers in atmospheric boundary layers under advective conditions differ considerably from those observed in areas over uniform surfaces. Airborne observations recently made in the coastal areas of the USG region showed, for instance, that under onshore wind conditions, the typical distribution of water vapour is plume-shaped and the latent heat fluxes are highest over land downstream of the water line (Shao and Hacker, 1990). Similar phenomena have also been observed in other studies. Figure 1 shows the humidity field and latent heat fluxes in the atmosphere over a desert lake (Lake Coongie, South Australia). Compared with the observations made in the USG region (see Figure 3 in Shao and Hacker, 1990), some common features are obvious. As dry air moved across the Lake (Gulf), its specific humidity increased as a result of evaporation. However, the water vapour was detained in a shallow layer over the lake and was mainly transported in the horizontal direction by the mean wind. Over land, with the development of convective turbulence, water vapour is rapidly dispersed upwards as indicated by the intense latent heat fluxes downstream of the lake (Figure 1b) and consequently the formation of the humidity plume. Farther inland, as the convective layer penetrated to higher levels, the depth of the humidity plume increased. Ohba and Nakamura (1990) performed wind tunnel

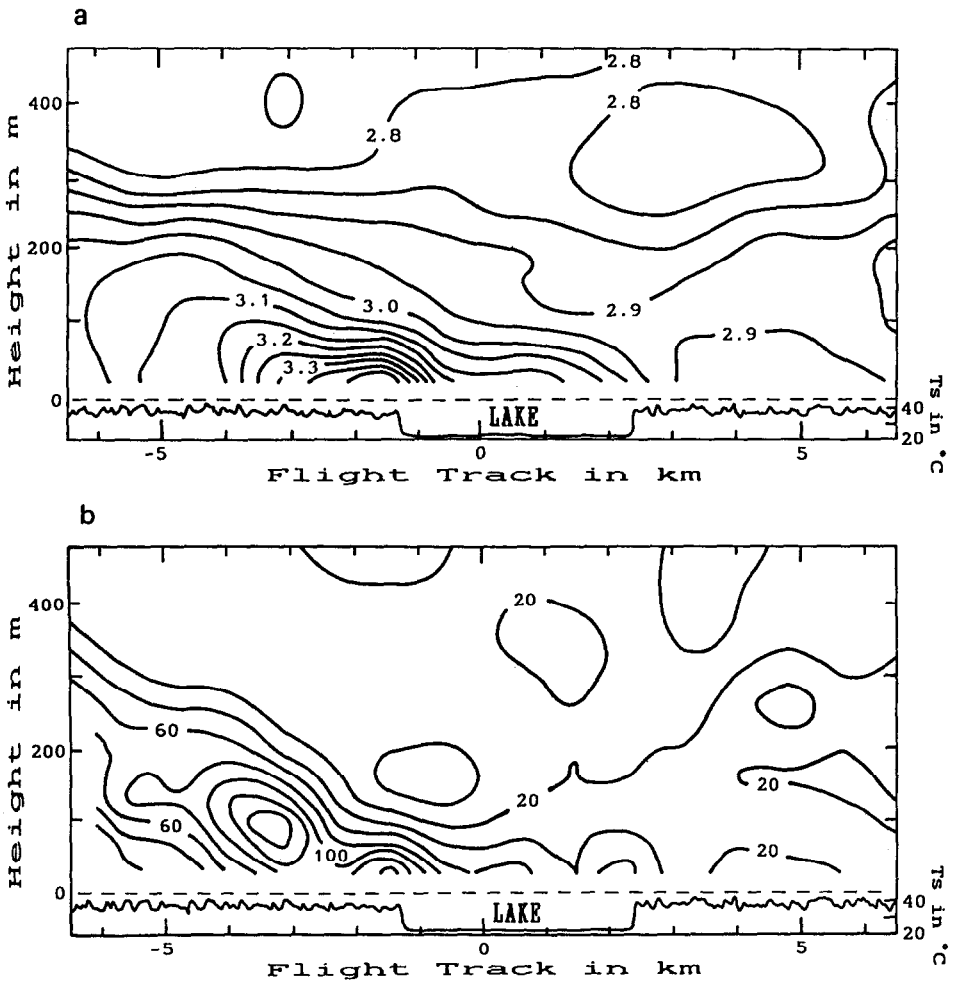

Fig. 1. Fields (west–east cross-sections derived from airborne obserations) of (a) specific humidity and (b) latent heat fluxes in the boundary layer over Lake Coongie of South Australia (redrawn from Hermsen, 1989). An easterly wind of about 5 m s^{-1} was measured during the airborne observations. Ts is surface temperature.

experiments for gas diffusion in coastal areas under neutral (Ri = 0, Ri is Richardson number), weakly unstable (Ri = −0.1) and moderately unstable (Ri = −0.6) conditions. They found that the distribution of tracer gas (CH_4) was plume-shaped with the plume axis ascending in unstable conditions as illustrated in Figure 2. These wind tunnel experiments show considerable similarity with the airborne observations presented in Figure 1.

3. The Lagrangian Dispersion Model

The basis of the Lagrangian approach is to simulate the trajectories of a representative sample of tracer particles in turbulent flows. Since the Reynolds number

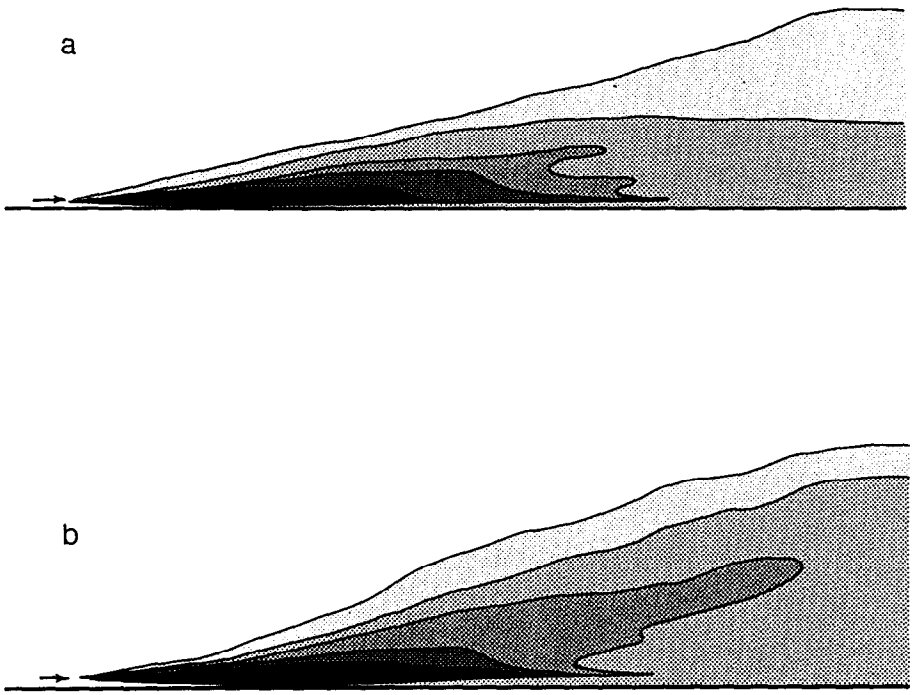

Fig. 2. Wind tunnel observations of smoke concentration for (a) weakly and (b) moderately unstable conditions. These illustrative graphs are redrawn from coloured photos of smoke plumes taken by Ohba and Nakamura using the laser sheet scattering method. Each tone level indicates an interval of concentration decreasing from dark to light tones (for detailed explanation, see Ohba and Nakamura, 1990).

in the atmosphere is large, molecular diffusion can be neglected and the tracer particles can be regarded as fluid elements. According to Thomson (1987), the velocity **U** and the position **X** of a fluid element are continuous functions of time t and their dynamic evolution can be considered as Markovian. Based on these two assumptions, the evolution of $(\mathbf{X}, \mathbf{U})$ can be described by (1). The random acceleration, $\mathrm{d}\xi_j$, is Gaussian white noise. The precise form of model (1), depending on the choice of b_{ij} and a_i, is constrained by Kolmogorov's theory of local isotropy and the requirement that it should reproduce given Eulerian velocity statistics.

Since $(\mathbf{X}, \mathbf{U})$ is assumed to be Markovian, model (1) describes the particle motions correctly on time scales larger than the Kolmogorov time scale τ_η only. According to Kolmogorov's theory of local isotropy (Monin and Yaglom, 1975, pp. 345–377), the Lagrangian structure function obeys

$$D_{ij} = \delta_{ij} C_0 \epsilon \, \mathrm{d}t \tag{2}$$

in the inertial subrange, where C_0 is a universal constant and ϵ is the dissipation rate for turbulent kinetic energy. By imposing this constraint of local isotropy at

small times (larger than τ_η but still within the inertial subrange) to model (1), it is obtained that

$$b_{ij} = \delta\sqrt{C_0\epsilon}\,. \tag{3}$$

The equivalent of Equation (1) in the Eulerian framework is the Fokker–Planck equation

$$\frac{\partial P_L}{\partial t} = -\frac{\partial U_i P_L}{\partial X_i} - \frac{\partial a_i P_L}{\partial U_i} + \frac{\partial^2 \frac{1}{2} b_{ik} b_{jk} P_L}{\partial U_i\, \partial U_j}\,, \tag{4}$$

where $P_L = P_L(\mathbf{X}, \mathbf{U}, t)$ is the probability density function of the phase-space distribution of tracer particles. The application of the Fokker–Planck equation in Lagrangian modelling is to determine a_i for given constraint on P_L. One of the criteria for the determination of a_i is the well-mixed condition, which requires that $P_L = P_E$ be maintained, P_E being the probability density function of the Eulerian velocity for given space and time. Thomson (1987) considered four other criteria and showed that they are either equivalent to, or less stringent than, the well-mixed condition. For model (1) to satisfy the well-mixed condition, it is necessary and sufficient that P_E should satisfy the Fokker–Planck equation. It follows that

$$a_i P_E = \frac{\partial \frac{1}{2} C_0 \epsilon P_E}{\partial U_i} + \phi_i\,, \tag{5}$$

where ϕ_i satisfy

$$\frac{\partial \phi_i}{\partial U_i} = -\frac{\partial P_E}{\partial t} - \frac{\partial U_i P_E}{\partial X_i}\,. \tag{6}$$

Hence, a_i can be obtained by solving the above equations under the condition $\phi_i \to 0$ as $U_i \to \infty$. If dispersion is in the vertical only, the Lagrangian model can be simplified to

$$\left.\begin{aligned} \mathrm{d}W &= a\,\mathrm{d}t + \sqrt{C_0\epsilon}\,\mathrm{d}\xi \\ \mathrm{d}Z &= W\,\mathrm{d}t \\ aP_E &= \frac{\partial \frac{1}{2} C_0 \epsilon P_E}{\partial W} + \phi \\ \frac{\partial \phi}{\partial W} &= -\frac{\partial P_E}{\partial t} - \frac{\partial W P_E}{\partial Z} \end{aligned}\right\}, \tag{7}$$

where W is the vertical velocity component, Z the vertical coordinate and for simplicity the suffixes for $\mathrm{d}\xi$ and ϕ are dropped.

For homogeneous stationary turbulence with no mean vertical flow, P_E is usually assumed to be Gaussian:

$$P_E = N(0, \sigma) \tag{8}$$

where

$$N(\alpha, \beta) = \frac{1}{\sqrt{2\pi\beta}} \exp(-\tfrac{1}{2}(W - \alpha)^2/\beta^2)$$

and σ is the standard deviation of the Eulerian vertical velocity. It can be easily shown that, for Gaussian turbulence, model (7) is identical to the classical Langevin-equation model (Lin and Reid, 1962; Gifford, 1982; Sawford; 1984)

$$\mathrm{d}W = -(W/T_L)\,\mathrm{d}t + (2\sigma^2/T_L)^{1/2}\,\mathrm{d}\xi\,, \tag{9}$$

where $T_L = C_0\epsilon/2\sigma^2$ is the Lagrangian time scale.

Turbulence in convective conditions, consisting of updrafts and downdrafts, is significantly non-Gaussian and inhomogeneous. Here, P_E can be constructed out of two Gaussian distributions (Thomson, 1984; van Dop *et al.*, 1985; de Baas *et al.*, 1986; Sawford and Guest, 1987)

$$P_E = pN(m_1, \sigma_1) + (1 - p)N(m_2, \sigma_2)\,, \tag{10}$$

where m_1 and σ_1 refer to mean and standard deviation of updrafts while m_2 and σ_2 to those of downdrafts; p represents the probability of updrafts; and $(1 - p)$ that of downdrafts. The first three moments are constrained by the corresponding statistic moments of the Eulerian velocity field. This leads to

$$\left.\begin{aligned} &pm_1 + (1 - p)m_2 = 0 \\ &p(m_1^2 + \sigma_1^2) + (1 - p)(m_2^2 + \sigma_2^2) = \sigma^2 \\ &p(m_1^3 + 3m_1\sigma_1^2) + (1 - p)(m_2^3 + 3m_2\sigma_2^2) = S_k\sigma^3 \end{aligned}\right\}, \tag{11}$$

where S_k is the skewness. These equations in the five unknowns p, m_1, m_2, σ_1 and σ_2 have two degrees of freedom, so two other requirements are chosen to simplify the arithmetic by imposing the conditions $m_1 = \sigma_1$ and $m_2 = \sigma_2$. It then follows from (11) that p, m_1 and m_2 must be

$$p = 0.5 - 0.5\sqrt{1 - 8/(8 + S_k^2)}\,, \tag{12}$$

$$m_1^2 = 0.5\sigma^2(1-p)/p\,, \tag{13}$$

$$m_2 = -m_1 p/(1 - p)\,. \tag{14}$$

Provided P_E is specified by (10), the solution for a can be found after some lengthy but simple calculations. It follows that

$$a = \left(0.5C_0\epsilon\frac{\partial P_E}{\partial W} + \phi\right)\Big/ P_E\,, \tag{15}$$

where

$$\frac{\partial P_E}{\partial W} = -\frac{pV_1}{\sqrt{2\pi\sigma_1^2}}\exp(-V_1^2/2) - \frac{(1-p)V_2}{\sqrt{2\pi\sigma_2^2}}\exp(-V_2^2/2)\,, \tag{16}$$

$$V_1 = W/\sigma_1 - 1\,, \tag{17}$$

$$V_2 = W/\sigma_2 + 1\,, \tag{18}$$

and

$$\begin{aligned}\phi = \frac{1}{\sqrt{2\pi}}\Bigg\{&\left[\sigma_1\frac{\partial p}{\partial Z} + p\frac{\partial \sigma_1}{\partial Z}\left(\frac{W^2}{\sigma_1^2}+1\right)\right]\exp(-V_1^2/2) + \\ &+\left[-\sigma_2\frac{\partial p}{\partial Z} + (1-p)\frac{\partial \sigma_2}{\partial Z}\left(\frac{W^2}{\sigma_2^2}+1\right)\right]\exp(-V_2^2/2)\Bigg\} - \\ &-0.5\Bigg\{\left[\sigma_1\frac{\partial p}{\partial Z} + p\frac{\partial \sigma_1}{\partial Z}\right][\mathrm{erf}(V_1/\sqrt{2})+1] + \\ &+\left[\sigma_2\frac{\partial p}{\partial Z} - (1-p)\frac{\partial \sigma_2}{\partial Z}\right][\mathrm{erf}(V_2/\sqrt{2})+1]\Bigg\}\,,\end{aligned} \tag{19}$$

where $\mathrm{erf}(x)$ is the error function. This formulation of the model is identical to that of Luhar and Britter (1989). The construction of the Lagrangian model is completed by specifying the Eulerian field of statistics, which must be externally specified from experimental studies. For homogeneous Gaussian turbulence, σ^2 and ϵ are required, while for inhomogeneous non-Gaussian turbulence, σ^2, ϵ and S_k need to be specified.

4. The Coastal Boundary Layer

Based on the experimental results presented in Raynor *et al.* (1979), Durand *et al.* (1989) and Shao (1990), the major features of the coastal boundary layer under onshore wind conditions can be summarised in Figure 3. When the water temperature is lower than the air temperature, the boundary layer over the water surface is stably stratified. Under onshore wind conditions, a convective sublayer, the thermal internal boundary layer (TIBL), develops over land due to the strong diabatic heating there. Turbulent fluctuations in the outer stable region are about 10 times weaker than those in the TIBL. Quantitative comparisons of turbulence statistics in the stable and convective regions of the coastal boundary layer can be found, for instance, in Shao and Hacker (1990). Turbulence in the stable region of the coastal boundary layer is shear driven and the probability density function is approximately Gaussian (Figures 3a, b). In contrast, turbulence within the TIBL is dominated by thermals and the probability density function is strongly non-

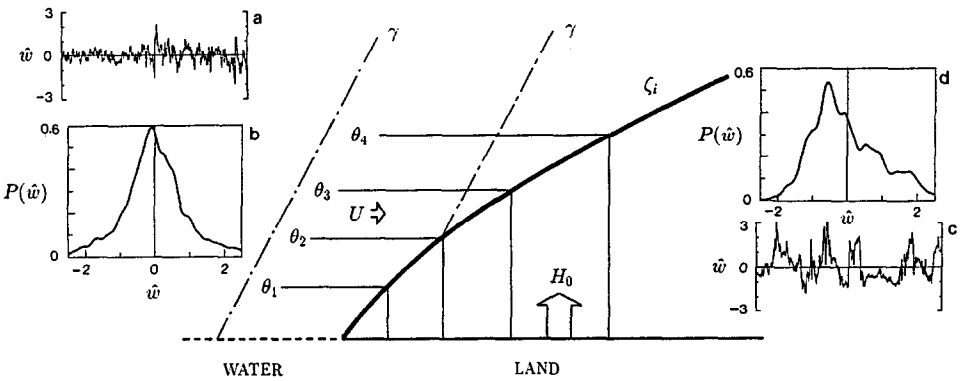

Fig. 3. A schematic illustration of the coastal atmospheric bounary layer under onshore wind conditions. (a) An example of normalized turbulent vertical velocity with its standard deviation ($\hat{w} = w'/\sigma$). (b) Probability density function for stable turbulence. (c) As (a), but for convective turbulence within the TIBL. (d) As (b), but for convective turbulence within the TIBL.

Gaussian with a positive skewness (Figures 3c, d). Similar to convective boundary layers over uniform surfaces, the TIBL has a layer of sensible heat fluxes and an entrainment layer. The height of the layer of positive sensible heat fluxes can be predicted by using Weisman's equation derived from the budget equation for sensible heat:

$$\zeta = \left(\frac{2H_0 x}{\rho C_p \gamma U_d}\right)^{1/2}, \tag{20}$$

where H_0 is the surface sensible heat flux over land, x the fetch, ρ the air density, C_p the specific heat of air at constant pressure, γ the static stability of the onshore airflow and U_d the depth-averaged onshore wind speed. Although the existence of the entrainment layer is widely accepted (Venkatram, 1977, 1986; Smedman and Högström, 1983; Durand *et al.*, 1989 and Shao *et al.*, 1991), the entrainment rate and the depth of such a layer is not well known. According to some observations available (Shao *et al.*, 1991), it is reasonable to assume that the TIBL depth ζ_i is approximately 1.2 times that of ζ.

Because of the transformation of boundary-layer mean structure and because turbulence properties vary both in the vertical and horizontal directions, it is expected that dispersion in coastal atmospheric boundary layers is more complex than in boundary layers over uniform surfaces. Tracer particles (water vapour) released from the water surface are initially dispersed in the vertical by homogeneous turbulence and transported onshore by the mean wind. Since turbulence in the stable region is weak, most of the particles are confined to a shallow layer until they move into the convective region over land, where they are dispersed rapidly upwards. Particles penetrating the upper boundary of the convective region again enter a stable region where they are subjected to Gaussian turbulence.

Therefore, the Lagrangian model must be able to simulate dispersion correctly in the stable region as well as in the convective region.

For the stable region of the boundary layer, Equation (8) can be used to specify the probability density function. For simplicity, the Eulerian variance of vertical velocity, σ^2 and the dissipation rate for turbulent kinetic energy, ϵ, are assumed to be constant. For the convective region of the boundary layer, the probability density function is specified by using (10). The spatial variation of turbulence statistics required by the Lagrangian model are those determined in Shao (1990), where it was shown that the characteristics of turbulence in the convective region of the coastal boundary layer depend only on three external parameters: the surface heat flux, the onshore wind speed and the stability of the untransformed airflow. The similarity relationships relevant for the present study are

$$\left.\begin{aligned} &\sigma^2/w_{*x}^2 = 2(z/\zeta_i)^{2/3}(1 - 0.8z/\zeta_i)^{3/2} \\ &\overline{w^{3\prime}}/w_{*x}^3 = 1.2(z/\zeta_i)(1 - z/\zeta_i) \\ &C_w\zeta_i^{2/3}/w_{*x}^2 = 1.3 + 0.1(z/\zeta_i)^{-1} \\ &w_{*x} = \left(\frac{g}{\Theta}\frac{H_0}{\rho C_p}\zeta_i\right)^{1/3} \\ &\zeta_i = 1.2\zeta \end{aligned}\right\}, \tag{21}$$

where w' is the turbulent vertical velocity, C_w the structure parameter of w' for the inertial subrange and z the height. The results are shown in Figure 4. These similarity relationships obtained for the TIBL have similar expressions to those obtained for homogeneous convective boundary layers, except that the scaling length ζ_i is a function of x. This can be interpreted as follows: the TIBL can be regarded as consisting of columns of air, the depth of which increasing in the onshore direction. The columns can be treated as well-mixed individually, and the turbulence properties are in equilibrium with the corresponding surface conditions. The results shown in Figure 4 indicate that mixed-layer scaling can be applied to these columns and their depth can be used as the scaling length. These columns are, however, not totally independent from each other and their mutual interaction depends on the advection of heat between them. It is in the scaling length, ζ_i, where the inhomogeneity effect is included in the scaling procedure, because the dependency of ζ_i on x is in principle determined by horizontal advection and vertical turbulent transport of sensible heat.

By using the relationships

$$C_w = 4\alpha\epsilon^{3/4}$$

$$S_k = \overline{w'^3}/\sigma^3,$$

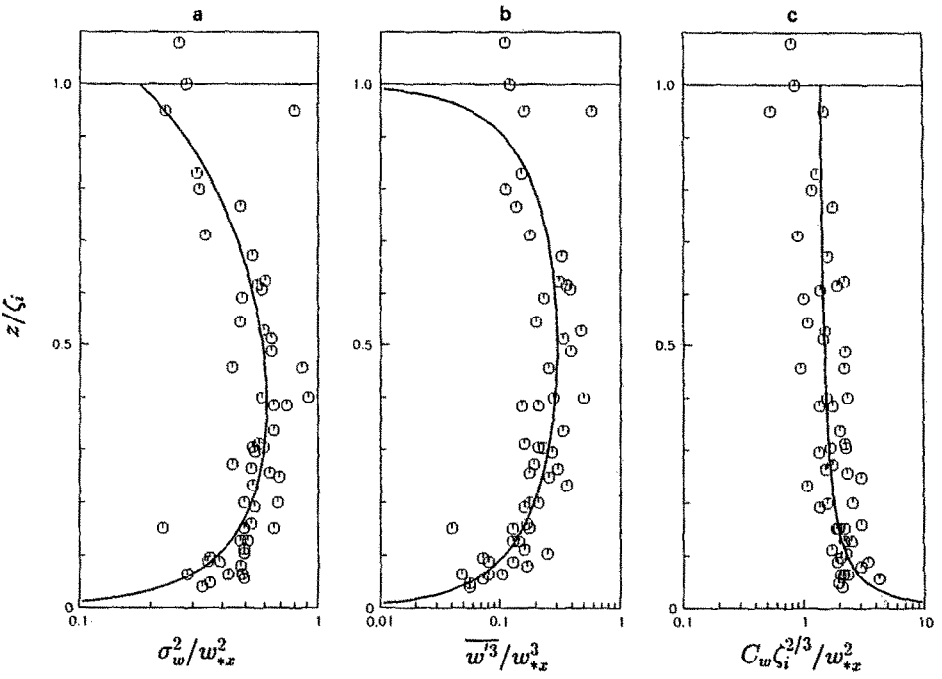

Fig. 4. (a) σ_w^2/w_{*x}^2 versus z/ζ_i. (b) $\overline{w'^3}/w_{*x}^3$ versus z/ζ_i. (c) $C_w\zeta_i^{2/3}/w_{*x}^2$ versus z/ζ_i. Open circles denote the observations obtained from the USG experiments. The curves correspond to the expressions given in (21).

where α is an universal constant of about 0.5, it is easily obtained

$$\left.\begin{aligned} \sigma &= \sqrt{2}w_{*x}(z/\zeta_i)^{1/3}(1-0.8z/\zeta_i)^{3/4} \\ S_k &= 0.42(1-z/\zeta_i)(1-0.8z/\zeta_i)^{-2} \\ \epsilon &= \frac{1}{\sqrt{8}}(1.3+0.1\zeta_i/z)^{3/2}w_{*x}^3/\zeta_i \end{aligned}\right\} . \tag{22}$$

The similarity relationships given by (22) are used in the Lagrangian model to classify the turbulence properties within the TIBL.

5. Dispersion in Convective Boundary Layers

The Lagrangian stochastic model is first applied to convective boundary layers over uniform surfaces and compared with other similar Lagrangian models and the well known laboratory observations of Willis and Deardorff (1976, 1978, 1981) using convective water tanks.

The similarity relationships

$$\frac{\sigma^2}{w_*^2} = 1.8\left(\frac{z}{z_i}\left(1-\frac{z}{z_i}\right)\right)^{2/3} + 0.2\left(\frac{z}{z_i}\left(1.25-\frac{z}{z_i}\right)\right)^{2/3}, \tag{23}$$

$$\frac{\overline{w'^3}}{w_*^3} = 0.96\frac{z}{z_i}\left(1-\frac{z}{z_i}\right) + 0.1\frac{z}{z_i}\left(1.25-\frac{z}{z_i}\right), \tag{24}$$

derived by Hartmann (1990) are used to specify the properties of turbulence in convective boundary layers, where z_i is the height of the inversion and w_* is the velocity scale for convective turbulence. The dissipation rate for turbulent kinetic energy is given by

$$\epsilon = 0.5 w_*^3 / z_i \,. \tag{25}$$

The initial velocity of the particles released at $z = z_s$ is assumed to have a Gaussian distribution, $N(0, \sigma_s)$, with σ_s set to $0.25\ \mathrm{m\,s^{-1}}$ as a rather arbitrary choice. A perfect reflection is imposed on the movement of the particles at the upper and lower boundaries. The number of particles released, N_0, is set to 20,000 which is generally sufficient to produce stable statistics. The mean particle concentration $\langle C \rangle$ and the vertical turbulent transport $\langle WC \rangle$ (see van Dop. *et al.*, 1985) are given by

$$\langle C(x,z)\rangle = Q/(N_0\,\Delta x\,\Delta z)\sum_{m=1}^{N_0}\int_0^\infty I_m(x,z,\Delta x,\Delta z,t)\,\mathrm{d}t\,, \tag{26}$$

and

$$\langle WC(x,z)\rangle = Q/(N_0\Delta x\,\Delta z)\sum_{m=1}^{N_0}\int_0^\infty WI_m(x,z,\Delta x,\Delta z,t)\,\mathrm{d}t\,, \tag{27}$$

respectively, where the indicator function I_m obeys

$$I_m = \begin{cases} 1 & \text{if particle at } t \text{ is at } (x \pm 1/2\Delta x, x \pm 1/2\Delta z)\,, \\ 0 & \text{otherwise}\,. \end{cases}$$

The average over all particles released from the source is represented by $\langle\ \rangle$ and Q is the source strength ($[Q] = \mathrm{g\,s^{-1}}$). The concentration is then normalised with Q/Uz_i, the flux with Qw_*/Uz_i and the vertical and horizontal position of the particles with z_i ($\tilde{Z} = Zz_i^{-1}$ and w_*/Uz_i ($\tilde{X} = w_*X/Uz_i$), respectively.

Figure 5 shows the fields of concentration for four different cases with z_s at 0.067, 0.24, 0.49 and $0.75z_i$. A comparison with the observations of Willis and Deardorff (1976, 1978, 1981) shows that this model reproduces the basic features found in the water-tank experiments. Figure 6 shows the mean particle height,

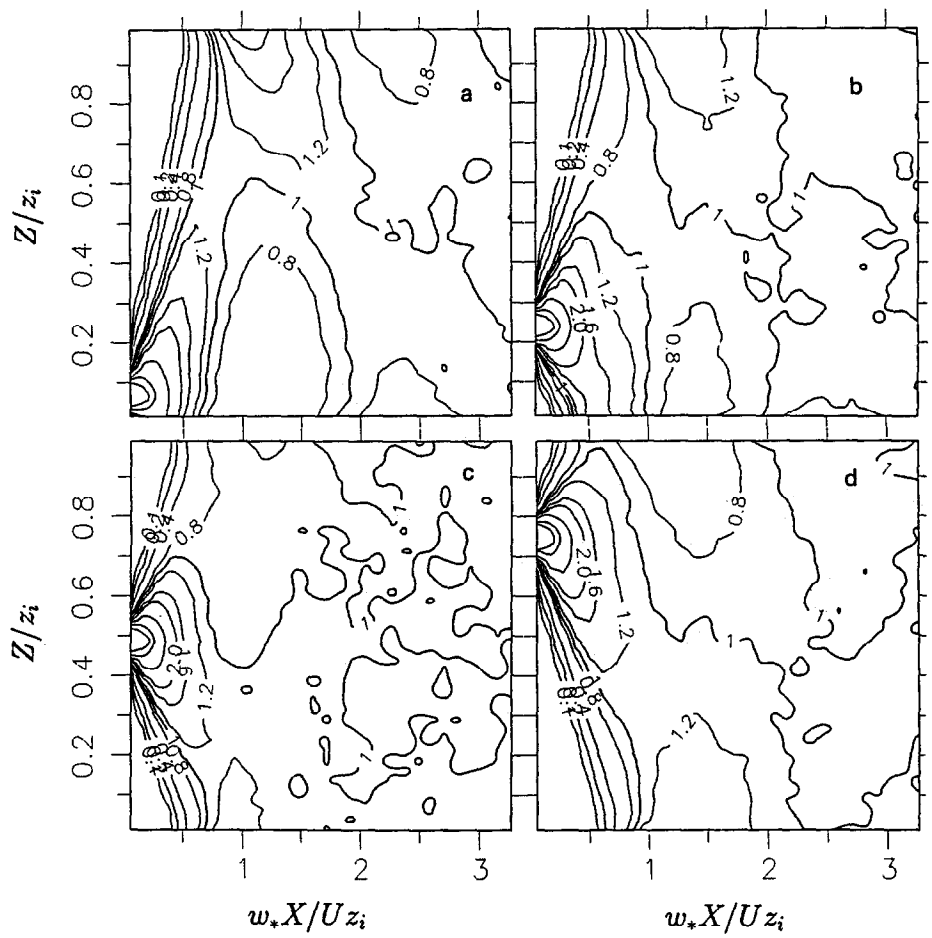

Fig. 5. Dimensionless concentration contours with source heights at (a) $0.067z_i$, (b) $0.24z_i$, (c) $0.49z_i$ and (d) $0.75z_i$.

$\langle Z\rangle/z_i$; the standard deviation, $\langle(Z - z_s)^2\rangle^{1/2}/z_i$; and the near surface concentration for the four different situations; these results agree with the corresponding quantities from the numerical simulations of Baerentsen and Berkowicz (1984), de Baas *et al.* (1986), Sawford and Guest (1987) and the laboratory observations of Willis and Deardorff (e.g., Figure 3 in Sawford and Guest). Contours of the normalised concentration flux are shown in Figure 7. Compared with the numerical simulation of previous studies (e.g., Figure 5 in Sawford and Guest), again an agreement between the simulations can be established. Based on these intercomparisons between models and laboratory experiments, it can be concluded that the model provides an adequate description of dispersion in convective boundary layers over uniform surfaces.

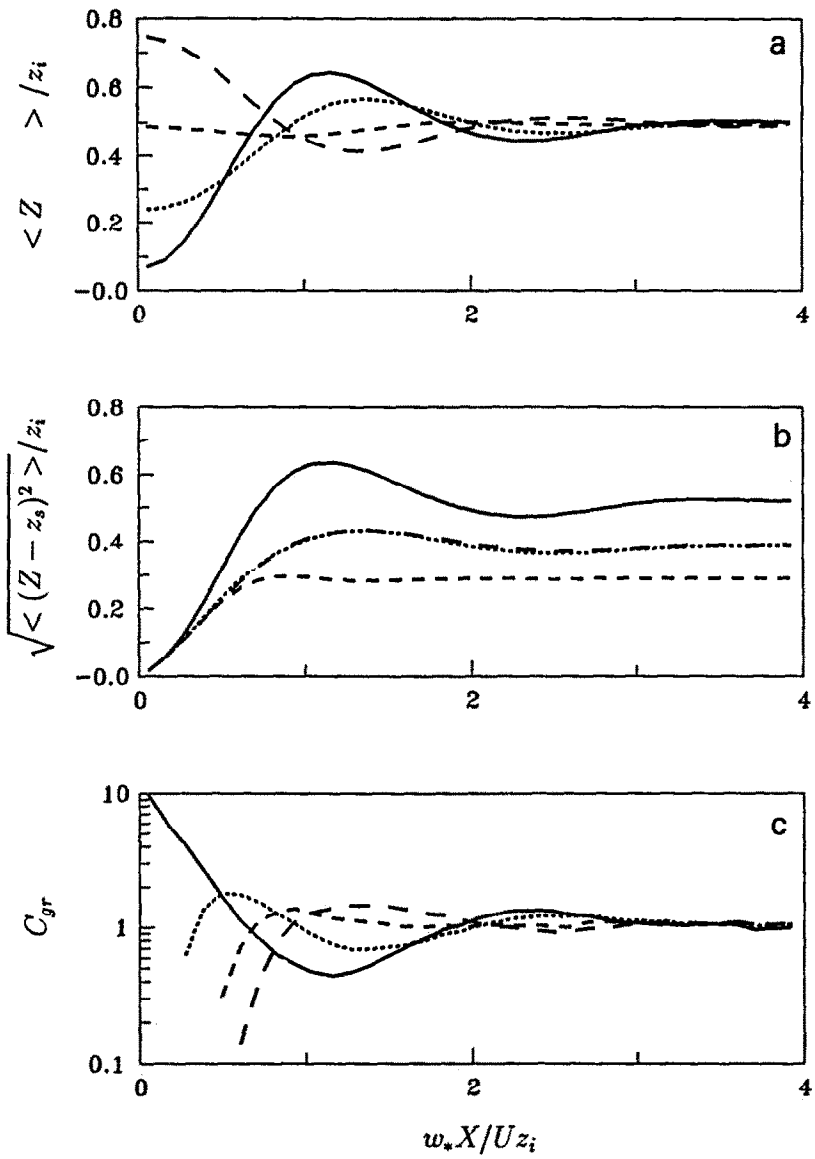

Fig. 6. (a) Mean particle height $\langle Z \rangle / z_i$, (b) standard deviation $\sqrt{\langle (Z - z_s)^2 \rangle}/z_i$ and (c) ground-level concentration C_{gr} as functions of $\tilde{X}$ for four different situations with z_s at 0.067, 0.24, 0.49 and $0.75 z_i$.

6. Dispersion in Coastal Boundary Layers

The Lagrangian model was next applied to study the dispersion of passive tracers in coastal areas. In the numerical simulation, the similarity relationships given by (22) are used to evaluate the evolution of turbulence within the TIBL while for simplicity, σ ($0.1\ \mathrm{m\,s^{-1}}$) and ϵ ($0.0005\ \mathrm{m^2\,s^{-3}}$) are assumed to be constant in the untransformed stable region. At the lower boundary, a perfect reflection is im-

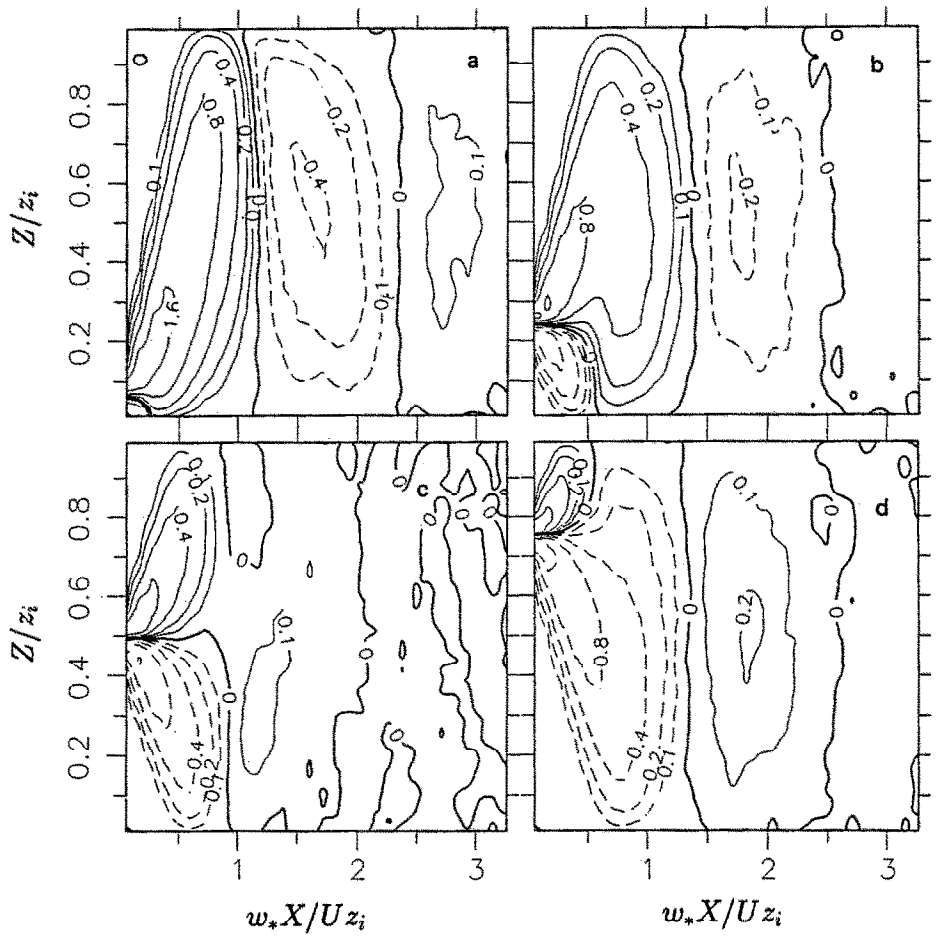

Fig. 7. Fields of concentration flux corresponding to the four different cases discussed in Figure 5.

posed on the particle motion although no upper boundary condition is applied. The lower boundary condition implies a zero flux of passive tracer at $z = 0, x \geq 0$. To simulate the dispersion of water vapour evaporated from the water surfaces, particles are randomly released from a line source (-5 km $\leq x \leq 0$) with the initial height of the particle randomly generated between 0 and 5 m.

External parameters H_0, γ and U_d need to be specified for the numerical simulation. These three parameters not only determine the depth of the TIBL but also the statistical properties of turbulence within this layer. It is thus expected that these parameters also determine the characteristics of dispersion. The influence of these parameters is discussed separately in the rest of this study. The choice of C_0 is also important for the outcome of the model. The exact value of C_0 is yet to be finalised. According to the experimental results of Hanna (1981) C_0 lies between 2 and 6. Sawford and Guest (1983) examined the behaviour of the model (1) for a simple inhomogeneous flow with different choices of C_0. They found that

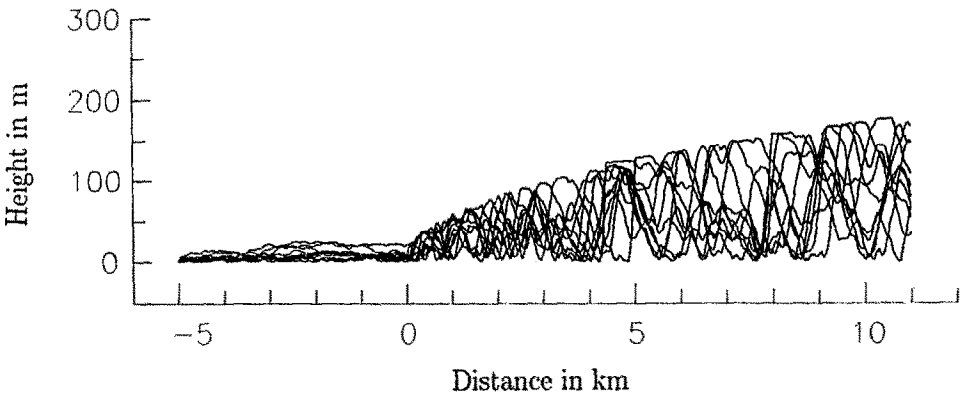

Fig. 8. Simulated trajectories of 10 particles released from a 5 km line source offshore ($x < 0$) for given external parameters.

for different values of C_0, set to 2.1, 5 or 10, the results of the simulation are significantly different. By comparing the results of the model with the study of Legg (1983) for a wind tunnel boundary layer, they found better agreement by choosing C_0 between 5 and 10. Thus, the choice of C_0 appears to require further investigations. In this study $C_0 = 5$ is used.

Examples of particle trajectories are presented in Figure 8, in which the movements of 10 particles are simulated for a given external situation. Because of the weak turbulence in the outer region of the coastal boundary layer, the particles released from the water surface are initially confined to a shallow layer. As they move into the convective region, the particles are rapidly dispersed in the vertical, showing the typical mixing effect of the convective turbulence. However, most of the particles are limited below the upper boundary of the TIBL, ζ_i. The movement of the particles reaching levels higher than ζ_i is again determined by the Gaussian turbulence there. As a consequence, these particles remain in the vicinity of ζ_i and most of them re-enter the convective region farther downstream.

The influence of H_0 on the dispersion is discussed in Figures 9 and 10. Figure 9 shows the fields of normalised concentration, together with the vertical tracer fluxes, for three different cases with H_0 equal to 100, 200 and 300 W m^{-2}, while Figure 10 shows the profiles of concentration and fluxes at different fetches. For the normalisation, the scaling length is set to $Z_r = 2000 z_0$, with z_0 (5 cm for this study) being the roughness height of the land surface. The scaling concentration is set to $C_s = Q/(U_d Z_r)$ and the scaling flux $F_s = w_s C_s$, where w_s is given by $w_s = (gH_0 Z_r/\rho C_p \Theta)^{1/3}$. For all three cases, U_d and γ are set to 4 m s^{-1} and 0.02 °C m^{-1}, respectively.

The basic features of the simulated concentration fields agree with the airborne observations made in Coongie Lake areas (Figure 1) and the wind tunnel experiment of Ohba and Nakamura (Figure 2). Figure 9 shows that, due to the weak turbulent activities in the stable region over the water surface, tracer particles (or water vapour) are detained initially in a shallow layer, causing a strong vertical

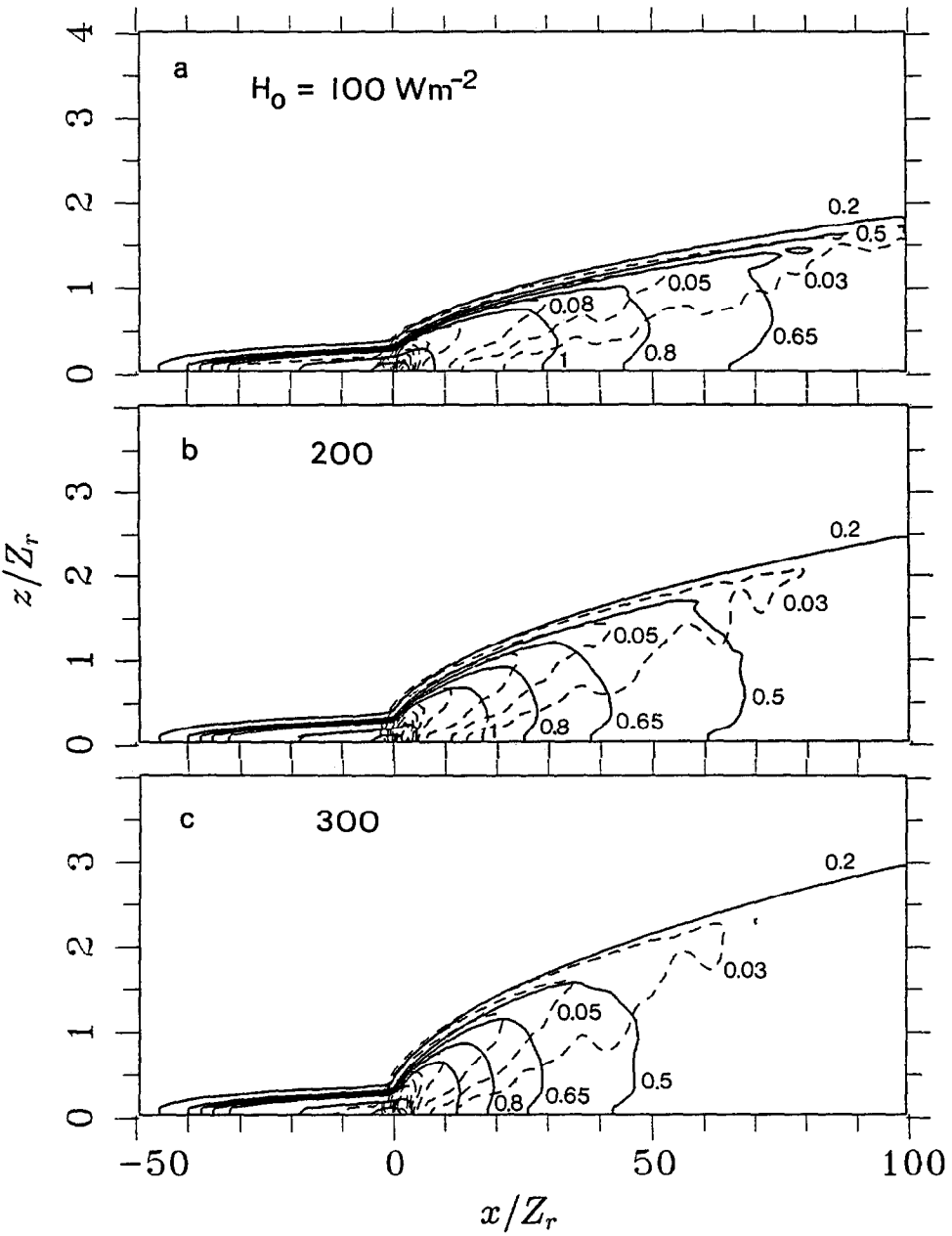

Fig. 9. Fields of concentration (solid line) and fluxes (dashed line) in normalised coordinates (x/Z_r, z/Z_r) for different values of H_0. For all three cases, $\gamma = 0.02\,^{\circ}\mathrm{C\,m^{-1}}$, $U_d = 4\,\mathrm{m\,s^{-1}}$ are used.

gradient of concentration. Advected into the convective region over land, particles are rapidly dispersed into higher levels and the concentration field becomes plume shaped. As can be seen from Figure 10, for a small distance onshore the concentration is highest in the middle of the convective region while that near the ground

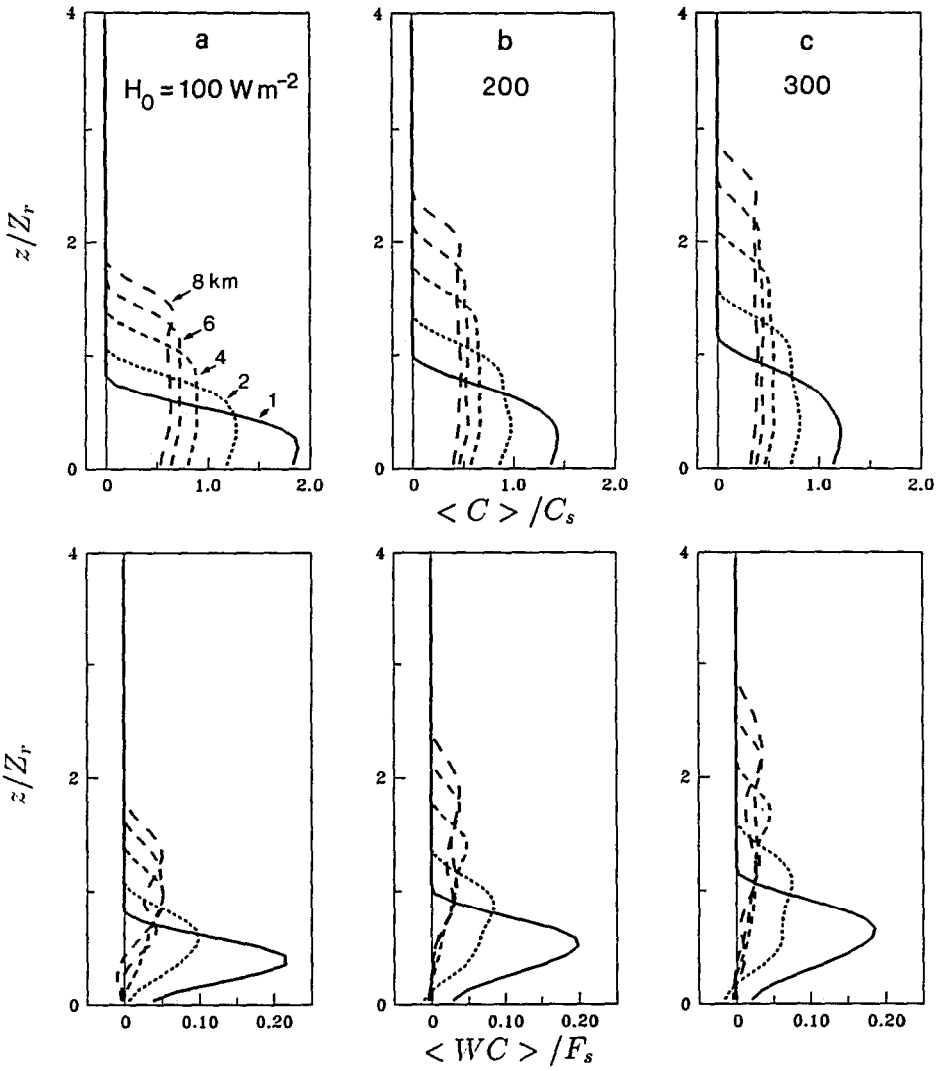

Fig. 10. Profiles of normalised concentration (above) and fluxes (below) at different fetches for the three cases discussed in Figure 9.

is relatively low. Farther inland, this tendency is diminished as a result of turbulent mixing and at a not too large distance onshore, a local equilibrium is reached with the particles evenly distributed (or well-mixed) with height in the TIBL as can be most clearly seen from Figure 10. The term "local equilibrium" is used because the mean concentration continues to decrease with fetch as the depth of the convective layer increases. In the case of small H_0 (Figure 9a), the tracer plume is flat, corresponding to a shallow TIBL; while for large H_0 (Figure 9c), the plume is steep corresponding to a deep TIBL. For large H_0 (Figures 9c, 10c), local equilibrium is reached at a small distance; and for smaller H_0, local equilibrium is reached at a larger distance from the source (Figures 9a, 10a).

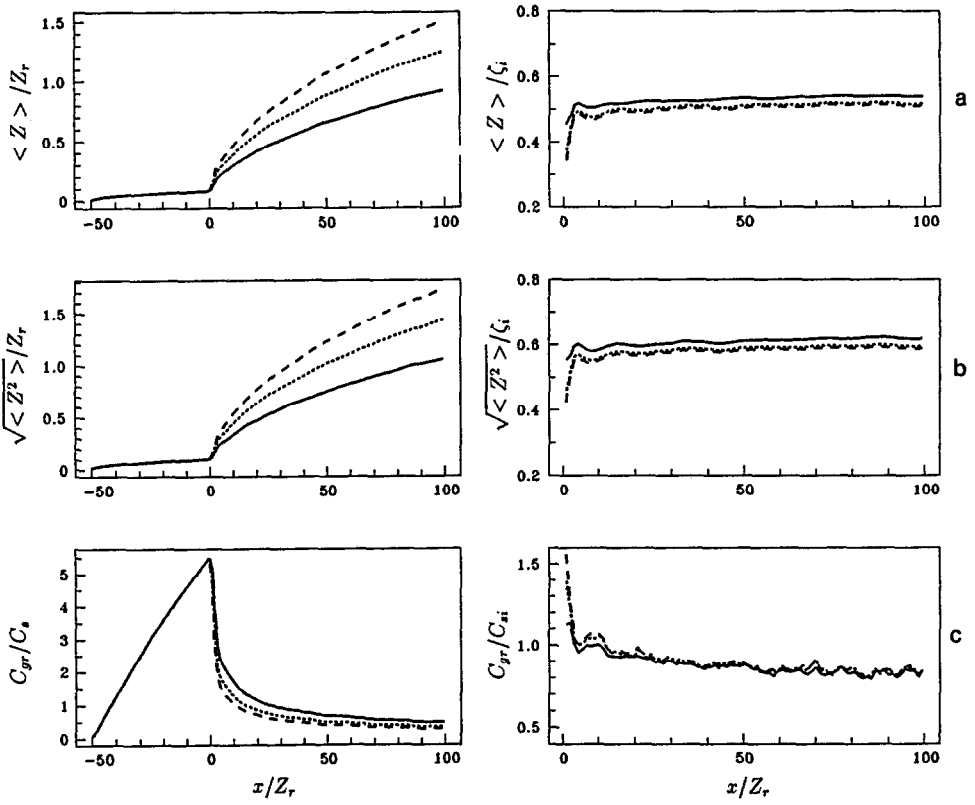

Fig. 11. Left: (a) mean particle height $\langle Z\rangle/Z_r$, (b) standard deviation $\sqrt{\langle Z^2\rangle}/Z_r$ and (c) ground-level concentration C_{gr}/C_s as functions of x/Z_r for three different cases in Figure 9. Right: (a) same as left but for $\langle Z\rangle/\zeta_i$, (b) $\sqrt{\langle Z^2\rangle}/\zeta_i$ and (c) C_{gr}/C_{si}.

The numerical simulation also reproduced the basic features of the vertical transport of passive tracers in coastal boundary layers. Figure 9 clearly shows that the maximum vertical tracer flux is located downstream of the water line for all three cases. Over land, the tracer flux first increases, then decreases with height. In the lower half of the TIBL, counter-gradient fluxes occur. All these features agree with the airborne observations shown in Figure 1. The model also shows that the maximum tracer flux without normalisation depends not only on source strength but also on the intensity of surface sensible heat flux over land. It can be shown that the maximum tracer flux for Figure 9c is twice as large as that for Figure 9a.

Figure 11 (left) shows the mean particle height $\langle Z\rangle$, the standard deviation $\sqrt{\langle Z^2\rangle}$ (both normalised with Z_r), and the near surface concentration C_{gr}, normalized with C_s. The mean particle height (Figure 11a) and the standard deviation (Figure 11b) increase with fetch in the convective region, and the rate of these increases is closely related to H_0. The simulation also shows that the surface concentration is highest at the coastline and decreases farther inland as a result

of increasing depth of the plume. The magnitude of C_{gr} decreases as H_0 increases. However, these three quantities have simple relationships with the depth of the TIBL, since the influence of H_0 on the dispersion is mainly manifested through its influence on ζ_i. As shown in Figure 11 (right), $\langle Z \rangle$ and $\langle Z^2 \rangle^{1/2}$ normalized with ζ_i, obtain a constant value of about 0.5 and 0.6 (except for a small distance near the coastline) and the differences between the three cases are not substantial. For C_{gr}, if normalized with $C_{si} = Q/U\zeta_i$ instead of C_s, the differences between the three cases are also insignificant. Compared with the dispersion of particles released from a ground-level source in convective boundary layers over uniform surfaces, it is obvious that $\langle Z \rangle/\zeta_i$ and $\sqrt{\langle Z^2 \rangle}/\zeta_i$ are similar to the equilibrium values of $\langle Z - z_s \rangle/z_i$ and $\sqrt{\langle (Z - z_s)^2 \rangle}/z_i$ shown in Figure 6.

The thermal stability of the onshore airflow also significantly influences the dispersion in the coastal boundary layer. Figure 12 shows three different situations with γ equal to 0.01, 0.02 and 0.04 °C m^{-1}. For all three cases, U_d and H_0 are equal to 4 m s^{-1} and 200 W m^{-2}, respectively. For a weakly stable onshore airflow (Figure 12c), the plume of tracer is steep with strong fluxes near the coast; while for a more stably stratified onshore airflow (Figure 12a), the plume is shallower and the vertical fluxes near the coast weaker. The third external parameter which affects the characteristics of dispersion in coastal areas is the onshore wind speed. However, it is obvious from (21) that an increase or a decrease of U_d has the same effects as an increase or a decrease of γ.

The application of the Lagrangian stochastic model can be easily extended to predict the dispersion of an air pollutant from an elevated source in coastal areas, which is of practical interest in environmental protection. Figure 13 presents an example of the concentration field and fluxes related to an elevated point source at Z_r, while Figure 14 shows the statistics of the plume. Again, in the stable region of the coastal boundary layer, the distribution and transport of the air pollutant show typical characteristics of Gaussian plumes. Here, the concentration is maximal at the source height and the dispersion of the pollutant can be described by Taylor's diffusion theory. In the convective region of the boundary layer, particles are rapidly dispersed to ground level as indicated by the significant negative fluxes (Figure 13) and increasing ground-level concentration. In this particular example, the maximum ground-level concentration is reached at a distance between 25 to 30 times the source height, but in general this distance can be estimated by

$$X_s = X_{s1} + X_{s2} .$$

In this expression, $X_{s1} = U_d \gamma \rho C_p h^2 / 3H_0$ is the distance recovered by tracer particles before hitting the upper boundary of the TIBL and $X_{s2} = U_d h / w_{*x}$ is approximately the distance traveled by tracer particles within the TIBL before hitting the ground. Farther downstream of X_s, the plume depth increases and the ground-level concentration decreases with fetch; these features of dispersion are similar to those related to ground sources.

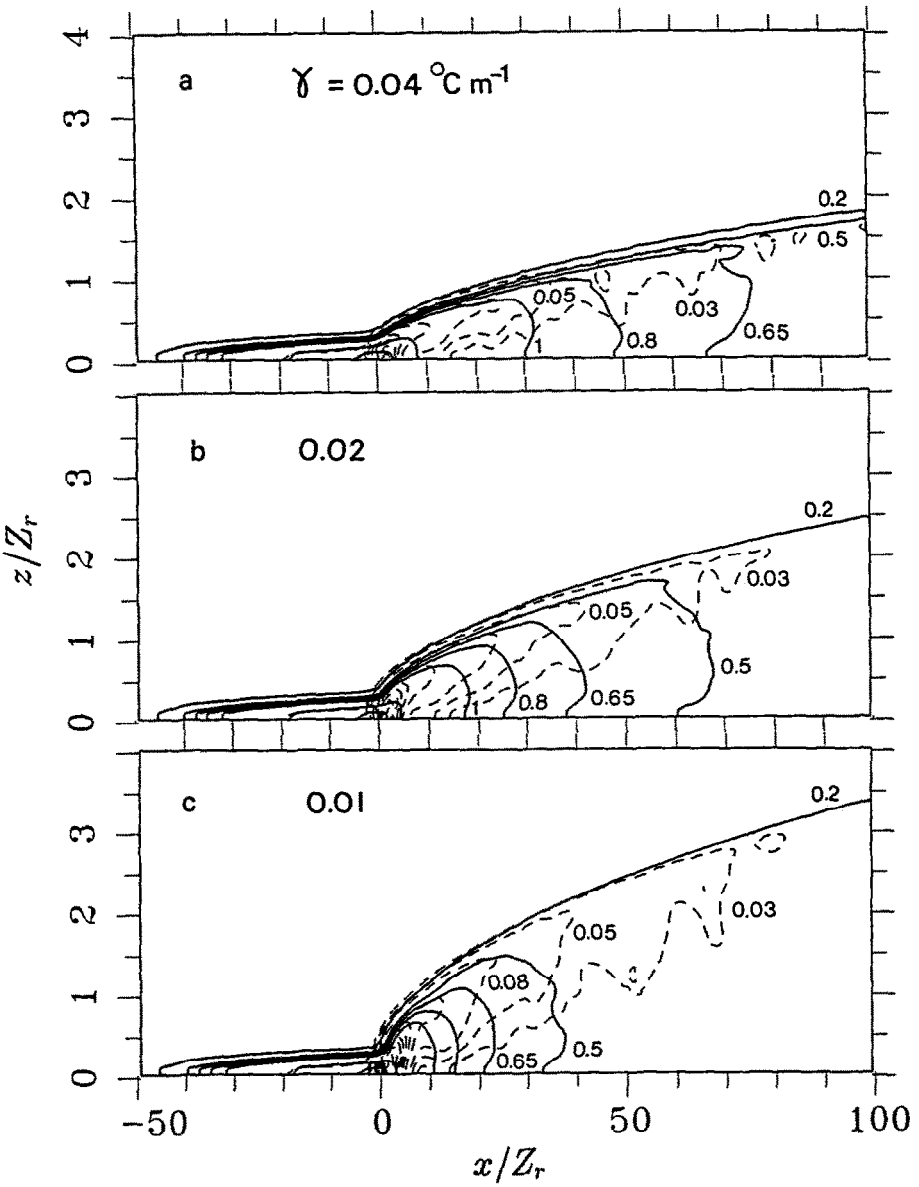

Fig. 12. Same as Figure 9 but for situations with different values of γ. For all three cases, $H_0 = 200\ \mathrm{W\ m^{-2}}$, $U_d = 4\ \mathrm{m\ s^{-1}}$ are used.

7. Summary

In this paper, the Lagrangian model suggested by Thomson (1987) was applied to simulate the dispersion of passive tracers in a coastal boundary layer under advective (onshore wind) conditions. The similarity relationships obtained in the USG experiments (Shao, 1990) were used to specify the statistical parameters used in

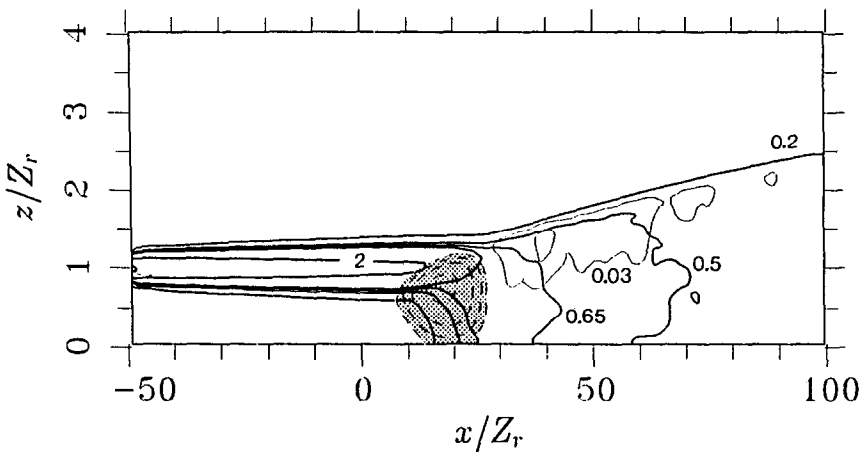

Fig. 13. Field of concentration (thick solid line) and fluxes (thin solid and dashed lines with the dashed lines in shaded area indicating negative fluxes) for an elevated point source at $z_s/Z_r = 1$.

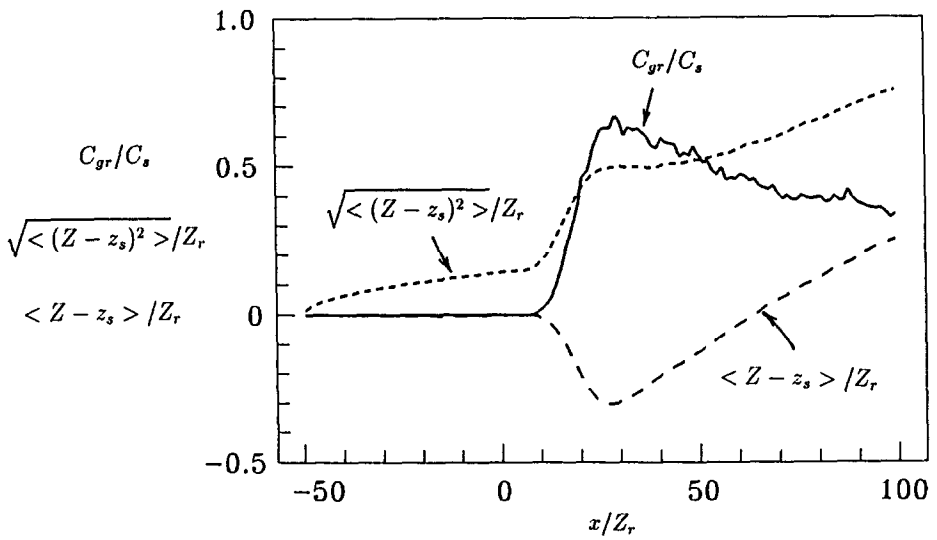

Fig. 14. Mean particle height $\langle Z - z_s \rangle / Z_r$, standard deviation $\sqrt{\langle (Z - z_s)^2 \rangle}/Z_r$ and ground-level concentration C_{gr}/C_s as functions of x/Z_r for the case discussed in Figure 13.

the model, such as the variance, skewness of vertical velocity and the dissipation rate for turbulent kinetic energy. Although the real situation was very much simplified in the model, it reproduced the fundamental features of the humidity field and the corresponding vertical latent heat transport recently observed in several coastal boundary-layer studies. The numerical simulation confirmed that the often observed humidity pool over cool water bodies is related to the stable structure of the turbulence, and the humidity plumes downstream of the coastline are related to the mixing effect of the convective turbulence and the development

of the TIBL. It revealed that large latent heat fluxes over dry land near the coast and counter-gradient fluxes in the low levels of the TIBL are a common feature of turbulent dispersion in coastal areas. Although the model was mainly applied to describe the dispersion of water vapour released from a surface source, the results are relevant for the dispersion of other passive tracers in boundary layers over nonuniform surfaces.

As a result of the numerical simulation, some features of turbulent dispersion in coastal boundary layers are now clear. It was shown that, except for a small distance onshore, a local equilibrium is reached when the particles become uniformly distributed in the vertical plane within the TIBL, while the concentration continued to decrease with fetch as a result of increasing depth of the tracer plume. The characteristics of dispersion in coastal areas are determined by H_0, γ and U_d, since these three parameters determine the behaviour of turbulence within the TIBL and its depth. As an application of the model, this paper examined the influences of H_0 and γ. It was shown that a large H_0 or a small γ (weakly stable onshore airflow) corresponds to a deep tracer plume and strong vertical transport; while for a small H_0 or a large γ, the tracer plume is shallow and the fluxes near the coast are weak. The influence of H_0 (also γ and U) on the dispersion of passive tracer was mainly manifested through its influence on the depth of the TIBL. It was shown that the mean particle position and depth of the plumes normalised with ζ_i are independent of H_0 and fetch, but have constant values of about 0.5 and 0.6. The concentration normalised with C_{si} was 0.3 to 0.9 near the surface and remained constant with height in the TIBL. Thus, the model indicated that a considerable amount of information can be obtained from the depth of the TIBL, which is in turn determined by H_0, γ and U_d.

Acknowledgements

I am grateful to Dr. B. Sawford for helpful advice regarding Lagrangian modeling and Dr. R. Ohba for kindly providing the photos from which Figure 2 was redrawn. A part of this study was done at the Flinders Institute for Atmospheric and Marine Sciences.

References

Baerentsen, J. H. and Berkowicz, R.: 1984, 'Monte Carlo Simulation of Plume Dispersion in the Convective Boundary Layer', *Atmos. Environ.* **18**, 701–712.

De Baas, A. F., van Dop, H., and Nieuwstadt, F. T. M.: 1986, 'An Application of the Langevin Equation for Inhomogeneous Conditions to Dispersion in a Convective Boundary Layer', *Quart. J. Roy. Meteorol. Soc.* **112**, 165–180.

Durand, P., Brière, S., and Druilhet, A.: 1989, 'A Sea-Land Transition Observed During the COAST Experiment', *J. Atmos. Sci.* **46**, 96–116.

Gifford, F. A.: 1982, 'Horizontal Diffusion in the Atmosphere: A Lagrangian Dynamical Theory', *Atmos. Environ.* **16**, 505–515.

Hanna, S. R.: 1981, 'Lagrangian and Eulerian Time-Scale Relations in the Daytime Boundary Layer', *J. Appl. Meteorol.* **20**, 242–219.

Hartmann, J.: 1990, 'Airborne Turbulence Measurements in the Maritime Convective Boundary Layer', Ph.D Thesis, Flinders University of South Australia.

Hermsen, P. A.: 1989, 'A Study of the Planetary Boundary Layer Structure over a Desert Lake from Airborne Observations', Honours Thesis, Flinders University of South Australia.

Legg, B. J.: 1983, 'Turbulent Dispersion from an Elevated Line Source; Markov Chain Simulation of Concentration and Flu Profiles', *Quart. J. Roy. Meteorol. Soc.* **109**, 645–660.

Lin, C. C. and Reid, W. H.: 1962, 'Turbulent Flow', in *Handbuch der Physik*, **VIII/2**, Springer, Berlin, pp. 438–523.

Luhar, A. K. and Britter, R. E.: 1989, 'A Random Walk Model for Dispersion in Inhomogeneous Turbulence in a Convective Boundary Layer', *Atmos. Environ.* **23**, 1911–1921.

Monin, A. S. and Yaglom, A. L.: 1975, *Statistical Fluid Mechanics*, Vol. 2, MIT Press, Cambridge, Massachusetts.

Ohba, R. and Nakamura, S.: 1990, 'Wind Tunnel Experiments on Gas Diffusion in Convection Layer', Proceedings American Meteorological Society, Ninth Symposium on Turbulence and Diffusion, April 30–May 3, 1990, RISØ, Roskilde, Denmark, pp. 367–370.

Raynor, G. S., Sethuraman, S. and Brown, R.: 1979, 'Formation and Characteristics of Coastal Internal Boundary Layers During Onshore Flows', *Boundary-Layer Meteorol.* **16**, 487–514.

Sawford, B. L.: 1984, 'The Basis for and Some Limitations of, the Langevin Equation in Atmospheric Dispersion Modelling', *Atmos. Environ.* **18**, 2405–2411.

Sawford, B. L. and Guest, F. M.: 1987, 'Lagrangian Stochastic Analysis of Flux-Gradient Relationships in the Convective Boundary Layer', *J. Atmos. Sci.* **44**, 1115–1165.

Sawford, B. L. and Guest, F. M.: 1988, 'Uniqueness and Universality of Lagrangian Stochastic Models of Turbulent Dispersion', Proceedings American Meteorological Society, 8th Turbulence and Diffusion Symposium, San Diego, April 25–29, pp. 96–99.

Shao, Y.: 1990, 'Turbulence and Turbulent Diffusion in a Coastal Atmospheric Boundary Layer', Ph.D. Thesis, Flinders University of South Australia.

Shao, Y. and Hacker, J.: 1990, 'Local Similarity Relationships in a Horizontally Inhomogeneous Boundary Layer', *Boundary-Layer Meteorol.* **52**, 17–40.

Shao, Y., Hacker, J. M. and Schwerdtfeger, P.: 1991, 'The Structure of Turbulence in a Coastal Atmospheric Boundary Layer', *Quart. J. Roy. Meteorol. Soc.* (in press).

Smedman, A. S. and Högström, U.: 1983: 'Turbulent Characteristics of a Shallow Convective Internal Boundary Layer', *Boundary-Layer. Meteorol.* **25**, 271–287.

Stunder, I. and Sethuraman, S.: 1985, 'A Comparative Evaluation of the Coastal Internal Boundar-Layer Height Equations', *Boundary-Layer Meteorol.* **32**, 177–204.

Thomson, D. J.: 1984, 'Random Walk Modelling of Diffusion in Inhomogeneous Turbulence', *Quart. J. Roy. Meteorol. Soc.* **110**, 1107–1120.

Thomson, D. J.: 1987, 'Criteria for the Selection of Stochastic Models of Particle Trajectories in Turbulent Flows', *J. Fluid Mech.* **180**, 529–556.

Van Dop, H., Nieuwstadt, F. T. M., and Hunt, J. C. R.: 1985, 'Random Walk Models for Particle Displacements in Inhomogeneous Unsteady Turbulent Flow', *Phys. Fluids* **28**, 1639–1653.

Venkatram, A.: 1977, 'A Model for Internal Boundary-Layer Development', *Boundary-Layer Meteorol.* **11**, 419–437.

Venkatram, A.: 1986, 'An Examination of Methods to Estimate the Height of the Coastal Internal Boundary Layer', *Boundary-Layer Meteorol.* **36**, 149–156.

Weisman, B.: 1976, 'On the Criteria for the Occurrence of Fumigation Inland From a Large Lake – A Reply', *Atmos. Env.* **10**, 172–173.

Willis, G. E. and Deardorff, J. W.: 1976, 'A Laboratory Model of Diffusion into the Convective Planetary Boundary Layer', *Quart. J. Roy. Meteorol. Soc.* **102**, 427–445.

Willis, G. E. and Deardorff, J. W.: 1978, 'A Laboratory Study of Dispersion from an Elevated Source Within a Modelled Convective Planetary Boundary Layer', *Atmos. Environ.* **12**, 1305–1311.

Willis, G. E. and Deardorff, J. W.: 1981, 'A Laboratory Study of Dispersion from a Source in the Middle of the Convective Mixed Layer', *Atmos. Environ.* **15**, 109–117.